ISSN 0021-3640, JETP Letters, 2017, Vol. 105, No. 9, pp. 577–581. © Pleiades Publishing, Inc., 2017.
Original Russian Text © S.P. Eliseev, N.S. Kurochkin, S.S. Vergeles, V.V. Sychev, D.A. Chubich, P. Argyrakis, D.A. Kolymagin, A.G. Vitukhnovskii, 2017, published in Pis'ma v Zhurnal Eksperimental'noi i Teoreticheskoi Fiziki, 2017, Vol. 105, No. 9, pp. 545–549.

OPTICS AND LASER PHYSICS

Purcell Effect in Triangular Plasmonic Nanopatch Antennas with Three-Layer Colloidal Quantum Dots

S. P. Eliseev[a, *], N. S. Kurochkin[a, b], S. S. Vergeles[a, c], V. V. Sychev[a, b], D. A. Chubich[a], P. Argyrakis[d], D. A. Kolymagin[a], and A. G. Vitukhnovskii[a, b, e]

[a] *Moscow Institute of Physics and Technology (State University), Dolgoprudnyi, Moscow region, 141700 Russia*

[b] *Lebedev Physical Institute, Russian Academy of Sciences, Moscow, 119991 Russia*

[c] *Landau Institute for Theoretical Physics, Russian Academy of Sciences, Chernogolovka, Moscow region, 142432 Russia*

[d] *Aristotle University of Thessaloniki, 54124 Thessaloniki, Greece*

[e] *National Research Nuclear University MEPhI (Moscow Engineering Physics Institute), Moscow, 115409 Russia*

**e-mail: elst@lebedev.ru*

Received February 15, 2017; in final form, March 29, 2017

A model describing a plasmonic nanopatch antenna based on triangular silver nanoprisms and multilayer cadmium chalcogenide quantum dots is introduced. Electromagnetic-field distributions in nanopatch antennas with different orientations of the quantum-dot dipoles are calculated for the first time with the finite element method for numerical electrodynamics simulations. The energy flux through the surface of an emitting quantum dot is calculated for the configurations with the dot in free space, on an aluminum substrate, and in a nanopatch antenna. It is shown that the radiative part of the Purcell factor is as large as 1.7×10^2. The calculated photoluminescence lifetimes of a CdSe/CdS/ZnS colloidal quantum dot in a nanopatch antenna based on a silver nanoprism agree well with the experimental results.

DOI: 10.1134/S0021364017090090

The interaction of light with metal nanoparticles may lead to the excitation of free-electron-cloud oscillations near the metal surface (localized plasmon resonance). Electromagnetic resonances associated with these excitations depend on the nanostructure topology and the conditions of their excitation, which opens broad prospects for the efficient control of optical processes on the nanosecond and picosecond time scales [1–3].

One example demonstrating the importance of research in laser nanoplasmonics is related to the ongoing pursuit of ever higher speed performance of nanodevices. The highest speed and smallest size of components used in different technologies are determined by the properties of the materials used, i.e., semiconductors (in electronics), dielectrics (in photonics), and metals (in plasmonics). One of the main current approaches to attaining further progress in the development of small-size (~10 nm) and, at the same time, high-speed (~10 THz) devices is based on nanoplasmonics.

The range of possible applications of nanoplasmonics utilizing both the near- and far-field zones is quite broad and includes plasmonic sensors [4, 5], multiphoton lithography [6], single-photon sources [7], plasmon lenses [8], "superabsorbers" [9], plasmon lasers [10], photovoltaic cells for solar power systems [11], and light-emitting diodes [12, 13]. One of the main elements that may find applications in nanoplasmonics is nanoantennas.

Work on nanoantennas begun in 1985, when John Wessel demonstrated the possibility of using metal nanoparticles as nanoantennas [14]. Nanoantennas may be monopole or dimer ones [15], the latter including, in particular, bowtie nanoantennas [16]. Much attention has been attracted recently to plasmonic nanopatch antennas, which consist of metal nanoparticles and metal films coated with a thin dielectric layer (dielectric spacer) [17]. Nanopatch antennas feature narrow radiation patterns [18], and, furthermore, their important advantage over dimer nanoantennas is the fact that high-precision electron-beam or ion-beam lithography is not required in the fabrication process for fine tuning of the gap between the metal nanoparticles.

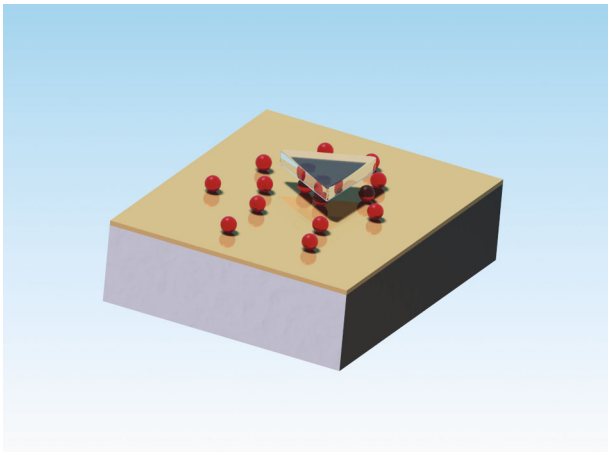

Fig. 1. (Color online) Three-dimensional model of a nanoantenna. The aluminum (lowermost) layer is coated with a layer of aluminum oxide (above the former), over which semiconductor emitters (quantum dots) are arranged. A triangular plasmonic silver nanoparticle is placed above the quantum-dot layer.

One of the main benefits of plasmon nanopatch antennas is the considerable increase in the rate of spontaneous emission. This effect is characterized by the Purcell factor [19]

$$F_P = \gamma_{sp}/\gamma_{sp}^0, \quad (1)$$

where γ_{sp}^0 and γ_{sp} are the rates of spontaneous emission of an emitter in free space and of the same emitter interacting with its environment, respectively.

The Purcell factor can also be defined via the ratio of the total power P_{tot} radiated by an emitter to the power P_0 radiated by the same emitter in free space as

$$F_P = P_{tot}/P_0, \quad (2)$$

because this ratio reflects the change in the number of excitation and spontaneous emission events per unit time.

The functioning of a plasmonic nanopatch antenna is accompanied by dissipative losses caused by the absorption of some fraction of radiation from the emitter in the metallic environment. These losses are characterized by the radiation efficiency ε_{rad}, defined as the ratio of the power P_{rad} radiated by the system in the far field to the total power P_{tot} radiated by the quantum emitter [20]:

$$\varepsilon_{rad} = \frac{P_{rad}}{P_{tot}}, \quad (3)$$

where the total power $P_{tot} = P_{rad} + P_{loss}$ is the sum of the radiated power and the loss power. The presence of these losses is frequently taken into account by introducing, in addition to the Purcell factor, its radiative part [19]:

$$F_P^{rad} = \frac{P_{rad}}{P_0}. \quad (4)$$

Patch nanoantennas with different shapes of plasmonic nanoparticles were considered in [21]. It was shown on the basis of numerical calculations that the largest Purcell factors can be obtained for triangular nanoparticles. For this reason, nanopatch antennas of this configuration were chosen in [22], where a 600-fold increase in the spontaneous emission rate γ_{sp} of CdSe/CdS/ZnS quantum dots was experimentally demonstrated.

The optical properties of nanopatch antennas are largely governed by plasmonic waveguide modes [23]. A key requirement for the observation of the Purcell effect is the enhancement of the interaction between excitons and electromagnetic field. This enhancement is caused by an increase in the field strength near the quantum dot owing to the excitation of a plasmon mode at the dipole-resonance frequency. Because of the dipole nature of this excitation, the effect of field enhancement decays quite slowly with distance (the field decreases by a factor 2 at a distance of about 10 nm) (see [24, 25]). The dipole plasmon peak depends considerably on the geometry of metal nanoparticles. In particular, the side length and the precision of the implementation of the corners have a strong impact in the case of a triangular prism [26].

Here, we numerically model the distribution of electromagnetic fields in nanopatch antennas fabricated using silver nanoprisms and spherical colloidal quantum dots based on cadmium chalcogenides. Modeling was carried out using the finite-element method. Special attention was paid to the calculation of the energy flux through the surface of quantum dots in different environments and of the power dissipated in silver nanoparticles and the aluminum layer.

The model of plasmonic nanopatch antenna was implemented using the Comsol Multiphysics software package and is schematically shown in Fig. 1. This model is formed by a 100-nm-thick aluminum layer coated with a 3-nm layer of aluminum oxide, over which one or several semiconductor quantum dots 10 nm in diameter and a triangular silver nanoprism are placed. We took the value of $\varepsilon_{QD} = 5.7$ for the dielectric constant of the quantum-dot material; this is a typical value for semiconductor structures based on CdSe, CdS, and ZnS. The dielectric constants of aluminum and aluminum oxide were taken from [27, 28]. The radiation of a quantum dot was modeled by that of a classical dipole located at its center and characterized by variable magnitude and direction of the dipole moment. The frequency of electromagnetic radiation was 4.8×10^{13} Hz, which corresponds to a vacuum wavelength of 630 nm. The height and side length of the nanoprism were 10 and 60 nm, respectively, and it was placed 10 nm above the surface of aluminum oxide.

The electromagnetic-field distribution was modeled on the basis of classical Maxwell's equations. In addition, we calculated the power dissipated in the silver nanoprism and in the aluminum layer. As an example, we show in Fig. 2 the distribution of the electric-field intensity in the plane parallel to the aluminum layer and passing through the center of a quantum dot located near a corner of the nanoprism. The dipole moment of the quantum dot is oriented along the z axis. According to this figure, the intensity of the electromagnetic field is highest near the nanoprism corners. Similar calculations of the electromagnetic-field distributions were carried out for an isolated quantum dot on a glass substrate and on an aluminum/aluminum oxide surface.

To determine the Purcell factor F_P, we calculated the integrated electromagnetic-energy flux P_{tot} through the surface of the quantum dot in four different configurations: a quantum dot on a glass substrate, on a two-layer aluminum/aluminum oxide surface, at the center of a plasmonic nanopatch antenna, and near a corner of the same antenna. The quantum emitter was modeled by a point dipole oriented along the z axis. The integrated fluxes, Purcell factors, dissipated powers, and radiation efficiencies are listed in Table 1.

The Purcell factor was calculated by Eq. (2). The energy flux through the surface of a quantum dot on a glass substrate was substituted here for the power P_0 emitted by the quantum dot in free space. The Purcell factors for the configurations with a quantum dot on an aluminum layer and at the center and near a corner of a nanoprism are 14, 72, and 1930, respectively (see table). Thus, the strongest enhancement in the photoluminescence rate occurs near the corners of a triangular nanoprism. The radiative part of the Purcell factor in this case is as large as 1.7×10^2.

The Purcell factors measured in our experimental study [22] for quantum emitters on aluminum and in a triangular plasmonic nanopatch antenna were 7 and 625, respectively. In that study, the quantum dots were randomly located and their dipoles were randomly oriented. Meanwhile, the calculations were carried out for fixed quantum-dot positions and orientations. We conclude that the calculated Purcell factors for a quantum dot on an aluminum layer and in a nanopatch antenna agree reasonably well with the experimental results.

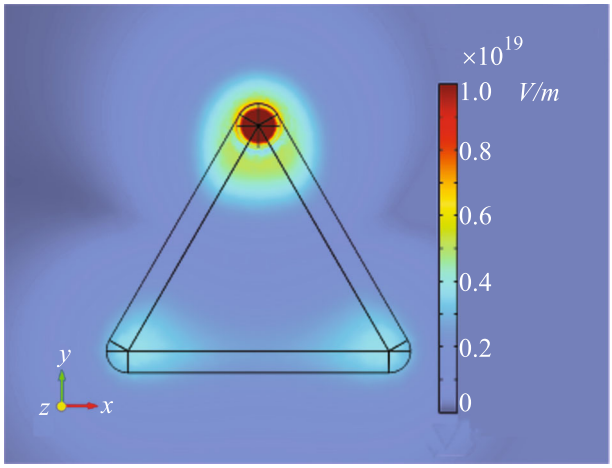

Fig. 2. (Color online) Outline of a plasmonic nanopatch antenna showing the map of the electric-field strength in the plane containing the center of the quantum dot and parallel to the aluminum layer. The color scale represents the amplitude of the electric-field strength (red color corresponds to the highest amplitude).

Figure 3 shows the calculated electric-field distributions for a nanopatch antenna with three quantum dots located at the corners of the nanoprism and characterized by different orientations of the dipole polarization. The highest intensity of the field is attained for a vertically polarized quantum dot. Thus, it may be supposed that the largest contribution to the Purcell effect in this nanopatch antenna comes from quantum dots with predominantly vertical orientation. Further-

Table 1. Integrated energy flux P_{tot} through the surface of the quantum dot, the Purcell factor F_P and its radiative part F_P^{rad}, the energy losses P_{loss}, and the radiation efficiency ε_{rad} for a quantum dot on glass, on an aluminum/aluminum oxide surface, and in a plasmonic nanopatch antenna at the center and near a vertex of a triangular nanoprism. The dipole moment of the quantum dot is oriented vertically (along the z axis)

Parameters	Quantum dot on glass	Quantum dot on Al	Quantum dot at the center of a nanopatch antenna	Quantum dot near a vertex of a nanopatch antenna
P_{tot} (arb. units)	3.25	4.68×10^1	2.33×10^2	6.26×10^3
P_{loss} (arb. units)	0	4.13×10^1	2.13×10^2	5.72×10^3
F_P	1	1.44×10^1	7.17×10^1	1.93×10^3
F_P^{rad}	1	1.69	6.15	1.66×10^2
ε_{rad}	1	0.12	0.09	0.09

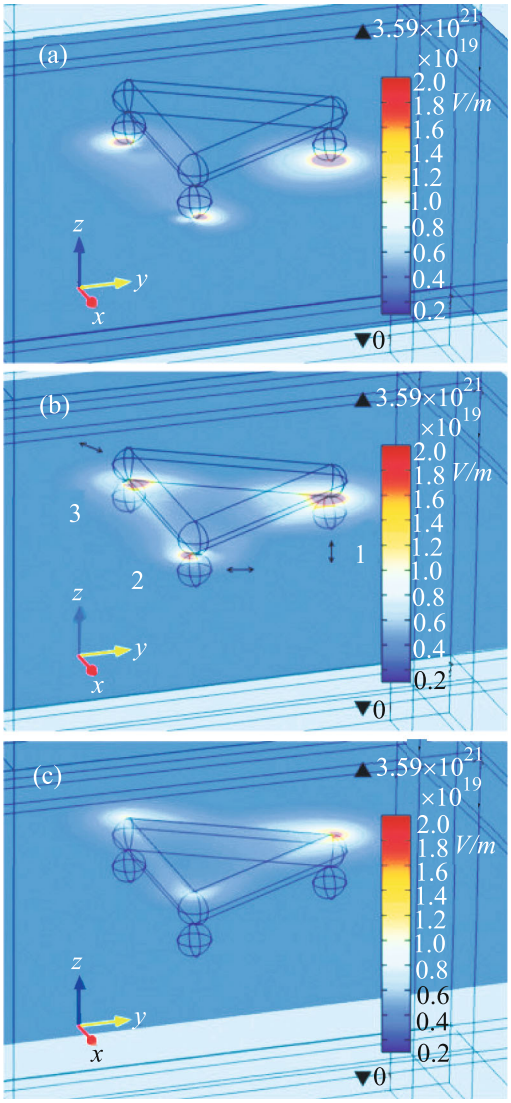

Fig. 3. (Color online) Calculated distributions of the electric-field strength in planes parallel to the xy plane. Quantum dots with different directions of the dipole polarization are arranged at the corners of the nanoprism. This direction is vertical (along the z axis), parallel to the y axis, and parallel to the bisector of the xoy angle for quantum dots 1, 2, and 3, respectively. The point dipoles are located at the geometric centers of the quantum dots. The planes are located at z = (a) 0.1, (b) 9.5, and (c) 20.0 nm ($z = 0$ corresponds to the air/aluminum oxide interface).

more, the results for quantum emitters corresponding to dots 2 and 3 (see Figs. 3a and 3b) indicate that, upon a shift from the oxide/air plane to the air/silver plane, there is a change in the field maximum, so-called "pole changeover" of the electric-field radiation pattern.

To summarize, we have numerically calculated the electromagnetic field distributions in nanopatch antennas of different configurations. We have found the effect of pole changeover in the electric field of quantum dots in the near-field zone. We have calculated the integrated radiation flux from the quantum dots and the power dissipating in the nanoantenna material. The Purcell factor has been calculated for an emitter on the top of a metal film and at the center and near the corner of a plasmonic nanopatch antenna. The calculated radiative part of the Purcell factor near a nanoprism corner is 1.7×10^2. The calculation results have been compared with the experimental data obtained by us earlier [22].

Work toward a more detailed understanding of the processes in the near-field zone of a nanopatch antenna and studies investigating the impact of the antenna shape and material on the characteristics of the emitted radiation are necessary for the optimal use of these components in various applications. The most important for applications is the possibility of real-time control over the spontaneous emission of a quantum dot in a nanopatch antenna using effects of the dynamic tuning of the plasmon resonance by an external electric field similar to that described in [29].

This work was supported by the Russian Science Foundation (project no. 15-19-00205). The use of the software was made possible by the Russian Foundation for Basic Research (project no. 16-29-11805).

REFERENCES

1. A. I. Dragan, E. S. Bishop, J. R. Casas-Finet, R. J. Strouse, J. McGivney, M. A. Schenerman, and C. D. Geddes, Plasmonics **7**, 739 (2012).
2. L. Lin and Y. Zheng, Opt. Lett. **40**, 2060 (2015).
3. B. Mali, A. I. Dragan, J. Karolin, and C. D. Geddes, J. Phys. Chem. C **117**, 16650 (2013).
4. C. Zhao, Y. Liu, J. Yang, and J. Zhang, Nanoscale **6**, 9103 (2014).
5. L. Shao, Q. Ruan, R. Jiang, and J. Wang, Small **10**, 802 (2014).
6. K. Ueno, S. Juodkazis, T. Shibuya, Y. Yokota, V. Mizeikis, K. Sasaki, and H. Misawa, J. Am. Chem. Soc. **130**, 6928 (2008).
7. R. Filter, K. Slowik, J. Straubel, F. Lederer, and C. Rockstuhl, Opt. Lett. **39**, 1246 (2014).
8. C. Ma and Z. Liu, J. Nanophoton. **5**, 051604 (2011).
9. Y. Cui, K. H. Fung, J. Xu, H. Ma, Y. Jin, S. He, and N. X. Fang, Nano Lett. **12**, 1443 (2012).
10. R. M. Ma, S. Ota, Y. Li, S. Yang, and X. Zhang, Nat. Nanotech. **9**, 600 (2014).
11. Z. Hu, J. C. Yu, T. Ming, and J. Wang, Appl. Catal. B: Environ. **168**, 483 (2015).
12. S. Schietinger, M. Barth, T. Aichele, and O. Benson, Nano Lett. **9**, 1694 (2009).
13. I. Gryczynski, J. Malicka, W. Jiang, H. Fischer, W. C. Chan, Z. Gryczynski, W. Grudzinski, and J. R. Lakowicz, J. Phys. Chem. B **109**, 1088 (2005).
14. J. J. Wessel, Opt. Soc. Am. B **2**, 1538 (1985).
15. O. Perez-Gonzalez, N. Zabala, and J. Aizpurua, Nanotechnology **25**, 035201 (2014).

16. J. Calderon, J. Alvarez, J. Martinez-Pastor, and D. Hill, Plasmonics **10**, 703 (2015).
17. C. Belacel, B. Habert, F. Bigourdan, F. Marquier, J. P. Hugonin, S. M. de Vasconcellos, X. Lafosse, L. Coolen, C. Schwob, C. Javaux, B. Dubertret, J. J. Greffet, P. Senellart, and A. Maitre, Nano Lett. **13**, 1516 (2013).
18. G. M. Akselrod, C. Argyropoulos, T. B. Hoang, C. Ciraci, C. Fang, J. Huang, D. R. Smith, and M. H. Mikkelsen, Nat. Photon. **8**, 835 (2014).
19. A. E. Krasnok, I. S. Maksymov, A. I. Denisyuk, P. A. Belov, A. E. Miroshnichenko, C. R. Simovskii, and Yu. S. Kivshar, Phys. Usp. **56**, 539 (2013).
20. V. Giannini, A. I. Fernandez-Dominguez, S. C. Heck, and S. A. Maier, Chem. Rev. **111**, 3888 (2011).
21. Z. Wu and Y. Zheng, Plasmonics **11**, 213 (2016).
22. S. P. Eliseev, A. G. Vitukhnovsky, D. A. Chubich, N. S. Kurochkin, V. V. Sychev, and A. A. Marchenko, JETP Lett. **103**, 82 (2016).
23. R. Alaee, C. Menzel, U. Huebner, E. Pshenay-Severin, S. Bin Hasan, T. Pertsch, C. Rockstuhl, and F. Lederer, Nano Lett. **13**, 3482 (2013).
24. V. V. Klimov, *Nanoplasmonics* (Fizmatlit, Moscow, 2010; Pan Stanford, Singapore, 2011).
25. J. E. Millstone, S. J. Hurst, G. S. Metraux, J. I. Cutler, and C. A. Mirkin, Small **5**, 646 (2009).
26. V. Klimov, G. Y. Guo, and M. Pikhota, J. Phys. Chem. C **118**, 13052 (2014).
27. K. M. McPeak, S. V. Jayanti, S. J. P. Kress, S. Meyer, S. Iotti, A. Rossinelli, and D. J. Norris, ACS Photon. **2**, 326 (2015).
28. R. Boidin, T. Halenkovic, V. Nazabal, L. Benes, and P. Nemec, Ceram. Int. **42**, 1177 (2016).
29. T. B. Hoang and M. H. Mikkelsen, Appl. Phys. Lett. **108**, 183107 (2016).

Translated by M. Skorikov